Research Article

Simultaneous Catalytic Oxidation of a Lean Mixture of CO-CH₄ over Spinel Type Cobalt Based Oxides

N. Neha*, Ram Prasad, Satya Vir Singh

Department of Chemical Engineering, Indian Institute of Technology (BHU), Varanasi 221005, India.

Abstract

A series of nickel-cobalt bimetal oxides in varying molar ratios and its single metal oxides were synthesized by reactive calcination of coprecipitated basic-carbonates. Several characterization techniques, such as: Bruneuer Emmett Teller (BET), X-ray Diffraction (XRD), Scanning Electron Microscopy (SEM), Fourier Transform Infra Red (FTIR), and Hydrogen Temperature Programmed Reduction (H₂-TPR), were performed over the oxides. Activities of oxides were evaluated in methane total oxidation in the presence or the absence of CO. The best catalytic performance was observed over NiCo catalyst with a Ni/Co molar ratio of 1:1, and the complete conversion of CO-CH₄ mixture was achieved at 390 °C. Moreover, the presence of carbon monoxide improves CH₄ total oxidation over nickel-cobalt mixed oxides. Structural analysis reveals that the insertion of nickel into the spinel lattice of cobalt oxide causes the structural disorder, which probably caused the increase of the amount of octahedrally coordinated divalent nickel cations that are responsible for catalytic activity. Stability of the best-performed catalyst has been tested in the two conditions, showing remarkable long-term stability and thermal stability, however, showed deactivation after thermally ageing at 700 °C. Copyright © 2020 BCREC Group. All rights reserved

Keywords: CO-CH₄ mixture oxidation; nickel cobaltite spinel; nickel-cobalt bimetal oxides; ageing

1. Introduction

International Energy Outlook report 2018 has forecasted the natural gas as fastest-growing source of energy next only to petroleum. The cleaner nature of natural gas as compared to oil or coal, as well as its non-controversial nature unlike nuclear energy, is expected to make it a fuel of choice for the recent future. Natural gas consists of 85-95% methane [1], which is the simplest hydrocarbon. The natural gas vehicles (NGVs) emit a much lower amount of harmful pollutants such as toxic non-methane hydrocarbons than those from conventional gasoline or diesel-powered vehicles [2].

However, NGVs also emit a significant amount of CO (~1.6%) and CH₄ (~0.4-1%) besides other pollutants like NOx and formaldehyde [3]. The health aspect of CO is that it avidly binds to hemoglobin in blood cells with an affinity of about 240 times that of oxygen [4], resulting in tissue hypoxia. Moreover, CO poisoning is often underdiagnosed as the clinical fea-

* Corresponding Author.
E-mail: n.neha.che14@itbhu.ac.in (N. Neha);
Phone: +91- 7860991830

tures of CO intoxication mimic very common conditions [5]. CO does not absorb terrestrial thermal Infra-red radiation strongly enough, thereby, not considered as a direct greenhouse gas. However, CO is an indirect greenhouse gas as it can influence the formation of the greenhouse effect. Methane is also a potent greenhouse gas with high global warming potential (GWP).

Thus, in the early 1970s, Europe started imposing emission norms limiting CO, HC, NOx, and PM. These regulations were based on European Union Research Organization (EURO) norms. Since the year 2000, India started imposing Bharat stage norms (BS norms), taking European norms as a reference and making these norms stricter with the need of time. Therefore, to meet the strict future emission norms, a lot of R & D work is going on worldwide to reduce emissions.

The low temperature of tailpipe exhaust (150-550 °C) demands the complete oxidation of CH_4 at this temperature itself. However, the strongest C-H bond (450 kJ/mol) in CH_4 among alkanes hinders its facile oxidative destruction at low temperature of tailpipe itself [6]. Thus, to decrease the required temperature for total CH_4 oxidation, catalytic oxidation is used. Additionally, as the non-catalytic oxidation of CH_4 occurs at high temperature (1500-2000 °C), it thermodynamically favor the formation of nitrogen oxides (NOx), whereas catalytic CH_4 oxidation occurs at much lower temperatures and thus generates much less amount of harmful NOx [7].

A noble metal-based catalyst exhibits an extraordinary catalytic activity for oxidation of CO [8] and CH_4 [9] at the low temperatures. Though, their high cost has led to the advancements in transition metal oxides (TMOs) synthesis as a practical alternative to noble metal-based catalysts owing to their low economic cost and high activity [10]. Among TMOs, Co_3O_4 is a homogeneous spinel with variable valence states (Co^{2+}, Co^{3+}, and Co^{4+}) of its cations is known to be very active for CO [11] as well as CH_4 oxidation [2]. Its outstanding catalytic activity is attributed to its weak M-O bond strength [12] and high turnover frequency (TOF) for redox reaction [2]. Meanwhile, NiO is also an important TMO having cubic lattice structure, contributes to the prominent defects such as cation vacancies and electron holes and thereby exhibits distinct magnetic, electronic, and catalytic properties [13,14].

Various researches in this field have demonstrated that the intrinsic activity of single oxide spinels such as Co_3O_4, can be further enhanced by substitution of Co^{2+} cations on the tetrahedral sites by other transition metal cations (*e.g.* Mn^{2+}, Ni^{2+}, Zn^{2+}, and Cu^{2+}), forming spinel mixed metal oxides or spinel bimetal oxides. This substitution enhances the catalytic performance owing to the presence of highly oxidized redox couples as well as the synergism between cations [3]. Junhua *et al.* [15] have reported the synergistic effect of Co-Mn spinel bimetal oxides and found that Co/Mn in the ratio of 5/1 shows the outstanding performance for methane oxidation owing to the best interaction among the metal ions at this ratio. The insertion of Mn into the spinel lattice of Co_3O_4 increases crystal defects, which lead to the enhancement in catalytic activity of the catalysts. Based on the previously published literature, it is anticipated that the appropriate mixing of NiO with Co_3O_4 can achieve outstanding catalytic activity for both methane and CO oxidation owing to their desirable intrinsic properties. Indeed, few studies on the individual oxidation of CO and CH_4 over nickel-cobalt mixed oxides have been reported in the literature. However, a study on the simultaneous catalytic oxidation of CO and CH_4 over Ni-Co mixed spinel oxides is not reported anywhere, even though this is a significant step towards practical environmental applications.

Further, various calcination parameters such as temperature [16], duration, and atmosphere (oxidative/reductive) are well known to influence the structural characteristics of a catalyst. Trivedi *et al.* [17] examined the influence of the calcination atmosphere on the catalytic performance of the catalysts. They found that the Mn-promoted Co_3O_4 spinel catalysts produced by reactive calcination (RC) form the oxygen-deficient highly active sites for CO-CH_4 oxidation. Such enthusiastic findings of our lab have motivated us to consider the RC route in our present study.

Thus, in this work, a series of Ni/Co bimetal oxides in the varied molar ratio were synthesized via co-precipitation technique, and the promotional effect of nickel on cobalt-based oxides was investigated. Additionally, the influence of CO (as reactant) on CH_4 oxidation was investigated. N_2 adsorption-desorption with BET method, XRD, FTIR, SEM, and H_2-TPR were used to examine the physiochemical and reducibility characteristics of the observed catalysts.

2. Materials and Methods

2.1 Catalyst Preparation

The Ni/Co bimetal oxide catalysts with var-

ying molar ratios of Ni to Co were synthesized via co-precipitation method following the procedure described by Junhua and co-workers [15]. All chemicals used in the preparation of the catalysts were of AR grade. The required amount of $Ni(NO_3)_2.6H_2O$ and $Co(NO_3)_2.6H_2O$, was dissolved in distilled water and mixed. Then, the mixed nitrate solution was added dropwise to the stoichiometric amount of Na_2CO_3 (2 M) aqueous solution with continuous stirring at 60 °C until pH reaches 9.3±0.01. The resulting precipitates were aged at 60 °C for 4h, then filtered and washed with warm distilled water several times, followed by drying at 100 °C overnight. The dried material was crushed and sieved to 40-60 mesh. The crushed precursor was reactively calcined (RC) and cooled in situ in the reactor in flowing reactive gas mixture of 4.5% CO in air. The detail of the RC method is described in next section 2.2 separately devoted to reactive calcination.

The catalysts with various Ni/Co ratios were designated as NiCo (molar ratio) in the manuscript. In addition, single oxides (NiO and Co_3O_4) were also prepared using respective nitrates and are reactively calcined before study of the reaction.

2.2 Reactive Calcination

Reactive calcination of the precursor was carried in situ in downflow bench-scale tubular reactor under atmospheric conditions in flowing reactive gas mixture consisting of 4.5% CO in air, flow rate of 40 mL.min^{-1}. The temperature was increased from room temperature at the rate of 2 °C.min^{-1} to a value where CO conversion was initiated; this temperature was maintained for a time till total CO conversion to CO_2 was observed. For the case of NiCo (1:1) precursor, this temperature was 160 °C and time required for 100% CO conversion was 32 minutes. After this, the temperature was increased to 500 °C, and the resultant catalyst was thermally annealed there for 2 h under the same reactive gas flowing conditions. In the beginning, at a constant temperature of 160 °C, very slow rate of oxidation of CO over the precursor's crystallites was observed, which caused an increase in the local temperature due to exothermic reaction. Such increase in local temperature started the slow decomposition of the precursor. Afterwards, slightly faster CO oxidation was observed due to the formation of crystalline structures which acted as a catalyst causing an increase in the rate of the oxidation process. During this period, the simultaneous occurrence of multifarious phenomenon of oxi-

dation - decomposition - redox - surface - reactions produced a synergistic effect which helps in the creation of oxygen-deficient active phases in the catalyst. The morphological characteristics attained by catalyst at low temperature found to remain intact at high-temperature conditions.

2.3 Catalyst Characterizations

X-ray powder diffraction patterns of the samples were recorded with an X-ray diffractometer (Rigaku Ultima IV, Germany) using nickel-filtered Cu-Kα radiation between 20° to 80° with continuous mode. The anode current and voltage were 250 mA and 40 kV, respectively. The mean crystallite size (d) of the phase was calculated from the line broadening of the most intense reflection using the Scherrer Equation (1).

$$d = \frac{0.89 \times \lambda}{\beta \times \cos\theta} \tag{1}$$

where 0.89 is the Scherrer constant, λ is the wavelength of the X-ray used (1.54056 Å), θ is the Bragg angle, and β is the effective linewidth of the observed X-ray reflection, calculated by the expression $\beta = B^2 - b^2$ where B is the full width at half maximum (FWHM), b is the instrumental broadening determined through the FWHM of the X-ray reflection at 2θ of crystalline SiO_2 for the instrument used ($b = 0.00274$).

The textural characterizations such as specific surface area and pore volume of the catalysts under study were examined by nitrogen sorption method (Micrometrics ASAP 2020) using liquid N_2 as adsorbent at its boiling point of -196 °C. BET surface areas of the samples were calculated from adsorption isotherm at a relative pressure range of 0.05-0.30. Before measurement, all the samples were degassed under vacuum conditions (10^{-6} torr) at 250 °C for overnight to make the surface clean for the sorption experiment.

Fourier transform infrared (FT-IR) absorbance spectra of the prepared catalysts was obtained on Shimadzu 8400 FTIR spectrometer from 400-4000 cm^{-1} using KBr pellets at ambient temperature. Micrographs were recorded on a high-resolution Carl Zeiss EVO 18 SEM instrument at an acceleration voltage of 15 kV and a work distance of 15 mm. Unless stated otherwise stated, 3000X magnification was used for all images.

Temperature programmed reduction by hydrogen (H_2-TPR) was conducted to examine the reducibility characteristics of the samples by

detecting the H_2 consumption. The H_2-TPR experiments were carried out in atmospheric pressure in a fixed-bed quartz reactor. Before experiments, the samples were pre-treated for 30 minutes under argon flow of 30 mL min^{-1} at 400 °C to remove the adsorbed moisture and other contaminants, followed by cooling to room temperature. After that, the reducing gas containing a mixture of 5%H_2 / 95%Ar at a flow rate of 40 mL.min^{-1} was passed over the samples (50 mg). The temperature was raised from room temperature to 650 °C at a heating rate of 10 °C.min^{-1}. The outlet stream was analyzed for H_2 by a TCD.

2.4 Catalytic Activity Measurement

The catalysts were evaluated for simultaneous oxidation of CO and CH_4 in a fixed bed continuous downflow tubular quartz reactor having an equivalent diameter 5.0 mm. The detailed description and dimensions of the reactor used in the study are mentioned elsewhere [18]. Being the exothermic nature of both CO and methane oxidation reaction, the catalysts were diluted with α-alumina (S_{BET} = 3.02 m^2.g^{-1}, pore volume = 0.01 cm^3.g^{-1}) to maintain the isothermal conditions in the bed under each steady-state observations. The following reaction conditions were maintained: 0.5 g of catalyst (35-60 mesh) (diluted to 1.5 mL with α-Al$_2$O$_3$), 1.5% CO + 1.5% CH_4 in 97% air and total flow rate of 100 mL.min^{-1}. Being the exothermic nature of both CO and methane oxidation reaction, the catalysts were diluted with α-alumina (S_{BET} = 3.02 m^2.g^{-1}, pore volume = 0.01 cm^3.g^{-1}) to maintain the isothermal conditions in the bed under each steady-state observations. The following reaction conditions were maintained: 0.5 g of catalyst (35-60 mesh) (diluted to 1.5 mL with α-Al$_2$O$_3$), 1.5% CO + 1.5% CH_4 in 97% air and total flow rate of 100 mL.min^{-1}. The uniform catalyst bed thickness was ensured to avoid any bypassing and axial dispersion [19].

The flow was controlled with the help of digital bubble gas flow meters at a GHSV of 60,000 h^{-1}. The air was made free of moisture and CO_2 by passing through a tower containing CaO and KOH. The reactor was placed vertically in a split open electrical furnace. The temperature of the catalyst bed was raised from room temperature to the temperature where total conversion of CO and CH_4 occurred with intermediate reactants conversions under steady-state conditions. The temperature was monitored and controlled using a K-type thermocouple placed in a thermo-well extended to the cat-

alyst bed. A microprocessor-based temperature controller with an accuracy of ±0.2 °C was used. The reactants and products gas compositions were analyzed by an on-line gas chromatograph (Nucon series 5765) equipped with Porapack Q-column, methanizer, and FID.

The catalytic activity for the simultaneous oxidation was calculated in terms of the conversion of limiting reactants such as CO and CH_4. The CH_4 conversion was calculated by the following Equation (2):

$$X_{CH_4} = \frac{\left[CH_4\right]_{in} - \left[CH_4\right]_{out}}{\left[CH_4\right]_{in}} \qquad (2)$$

Meanwhile, the conversion of CO-CH_4 mixture was measured on the using values of the concentration of CO_2 in the product stream by the following Equation (3):

$$X_{(CO+CH_4)} = \frac{\left[CO_2\right]_{out}}{\left[CH_4\right]_{in} + \left[CO\right]_{in}} \qquad (3)$$

2.5 Catalyst Stability Test

The life of a catalyst is a significant factor in examining the overall performance of the catalyst. The thermal sintering of a catalyst is a major cause of irreversible catalyst deactivation. Therefore, the stability test on the best-performed catalyst was performed in the reaction environment by employing two different methods. These tests were conducted at the optimum GSHV necessary to achieve the maximum conversion, *i.e.* 60,000 h^{-1} so that the deactivation would not be hidden because of the presence of excess of active sites. The methods are as follows:

Time on stream run test: The time on stream experiment was conducted for the best-performed catalyst to observe the influence of time on the catalyst performance at a constant temperature under reaction conditions. The oxidation of CO-CH_4 mixture was conducted at 390 °C corresponding to the total oxidation of reactants for 50 h, with hourly measurement of reactants conversions.

Thermal ageing tests: These tests are simulation of ageing occurring due to a complex set of physical and chemical changes during the lifetime of the catalyst. Various factors such as prevalence of lower flame speed, long engine running hours and fuel shut off conditions results in higher temperature of CNG engine exhaust [20]. Thermal ageing is a consequence of these high-temperature surges in the exhaust control systems. The rapid deactivation of TWC due to thermal and chemical ageing is observed on CNG fueled vehicles than on gasoline fueled

ones [21]. Therefore, thermal ageing tests were conducted by ageing the catalysts at the targeted temperature to examine the influence of ageing on their respective catalytic performances. Aged catalysts were obtained by treating fresh ones in muffle furnace at 500, 600, and 700 °C for overnight period. The ageing temperatures were above the normal operating temperature of the catalysts in the converter. The performance tests of such aged catalysts were conducted as discussed under the previous Section 2.4.
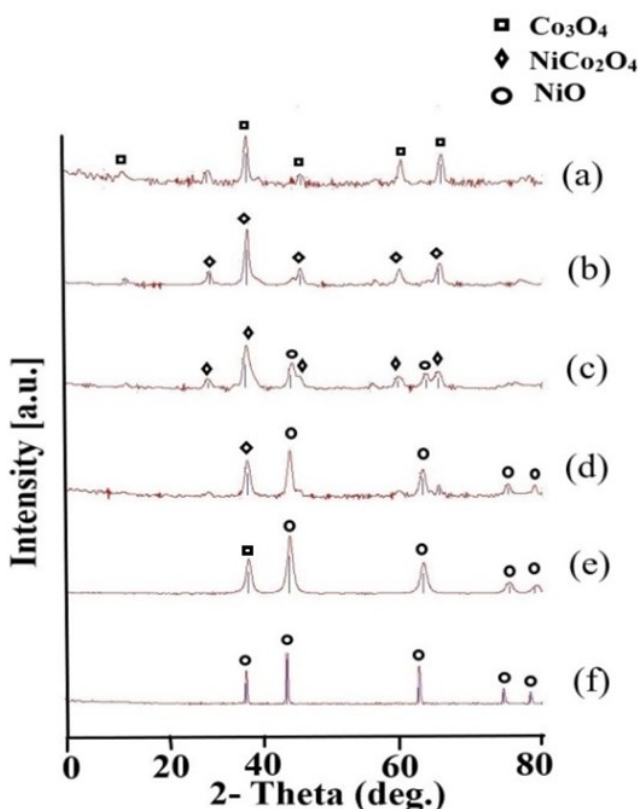
3. Results and Discussions

3.1 XRD results

The XRD patterns of all the samples are shown in Figure 1. The peaks in XRD patterns of NiO and CO_3O_4 samples are accurately assigned to NiO phase (JCPDS 47-1049) and Co_3O_4 phase (JCPDS 43-1003), respectively. For the case of Ni-Co containing oxides (b-e), both $NiCo_2O_4$ phase (JCPDS 20-0781) and NiO phase exist together except for the case of Ni/Co molar ratio of 1:2. For NiCo (1:2) single phase of $NiCo_2O_4$ appeared. The lattice parameters (a) and the crystallite size (d) are summarized in Table 1. The gradual shift in the diffraction peak toward low 2θ angle is observed with increasing Ni content from Ni/Co molar ratio of 1:2 to 1:1. The NiCo (1:1) and (1:2) sample are largely shifted to a lower angle, indicating the substitution of the smaller Co^{3+} (r = 0.055 nm) ions with larger Ni^{2+} (r = 0.069 nm) ions preferring the octahedral sites in Co_3O_4 spinel lattice. Further, it was observed that in the case of samples corresponding to the Ni/Co molar ratio of 1:2 and 1:1, comparatively broad and low-intensity peaks were observed indicating a low degree of crystallinity and small size of a crystalline grain. However, when Ni/Co exceeds 1:1 molar ratio, such as in case of NiCo (2:1) and single NiO, the peak intensity again gets increased and crystalline NiO phase starts dominating, resulting in the large average size of crystalline grains. The number of crystal defects such as the formation of distorted spinel lattice in case of Ni-Co (1:1) may get increased with the insertion of Ni into the spinel lattice of cobalt oxide. Hence, the noteworthy factors such as less crystallinity, small average crystallite size, and distorted spinel phase in case of samples such as NiCo (1:1) can be accountable for its desirable characteristics.

Figure 1. XRD patterns of (a) Co_3O_4, (b) NiCo (1:2), (c) NiCo (1:1), (d) NiCo (2:1), (e) NiCo (1:1) aged at 700 ºC, and (f) NiO.

Table 1. Lattice parameters (a), crystalline sizes (D), S_{BET} and pore volume values of the catalysts.

Cat	NiO	$NiCo_2O_4$		Co_3O_4		S_{BET}	Pore Volume
	a^a (Å)	a^a (Å)	D (nm)	a^a (Å)	D (nm)	(m² g⁻¹)	(cm³g⁻¹)
Co_3O_4	-	-	-	8.061	23.02	46.1	0.26
NiCo(1:2)	4.177	8.120	12.2	-	-	55.5	0.28
NiCo(1:1)	4.16	8.125	10	-	-	65.5	0.33
NiCo(2:1)	4.183	8.111	11	-	-	46.7	0.26
NiO	4.179	-	-	-	-	41.2	0.21
NiCo aged	4.180	8.110	19.9	-	-	-	-

[a]Calculated by fitting the XRD patterns using MAUD Rietveld refinement program

## 3.2 BET Characterization Results

The textural properties, such as: S_{BET} and pore volume results of all the samples, are given in Table 1. The S_{BET} and pore volumes values in case of single oxides (NiO and Co_3O_4) were found to be same, indicating that these two single oxides have somewhat identical textural properties. The S_{BET} and pore volume exhibited by NiCo bimetal oxides is significantly higher than their single oxides. The surface ar-

eas and pore volume of the samples found to be increased with the increase in Ni content till the NiCo (1:1) then again decreased to the value of single oxide NiO. The NiCo (1:1) catalyst has shown the highest S_{BET} (65.5 $m^2.g^{-1}$) and the largest pore volume (0.33 $cm^3.g^{-1}$) among all the observed catalysts. Previous works [15,22,23] on mixed metal oxides has also reported that mixed metal oxides have higher specific surface areas than their single oxides.

3.2 FT-IR Characterization Results

The IR-spectra of all the samples are shown in Figure 2. In single NiO (Figure 2e), strong band was observed at 420 cm^{-1} corresponding to the vibration of Ni-O bond [13]. In the case of cobalt-containing metal oxides (a-d), two most intense bands appear in about 518 and 660 cm^{-1} region. These two transmittance bands correspond to the M-O stretching vibrations from tetrahedral and octahedral sites, respectively, are characteristic of spinel structure. As can be observed in Figure 2, the peak positions were shifted slightly to the lower wavelength with the increase in Ni oxide content [24]. Peak shifting and signal enhancement in Ni-Co based samples can be attributed that the interaction between two phases results in more structure distortions.

The broad absorption band around 3321 cm^{-1} corresponds to the O-H stretching vibrations, indicating that fact that the calcined
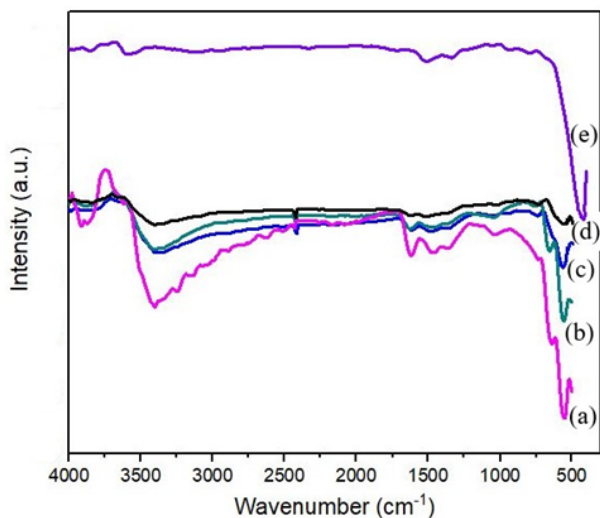
Figure 2. FT-IR spectra of (a) NiCo (2:1), (b) NiCo (1:1), (c) NiCo (1:2), (d) Co_3O_4, and (e) NiO.
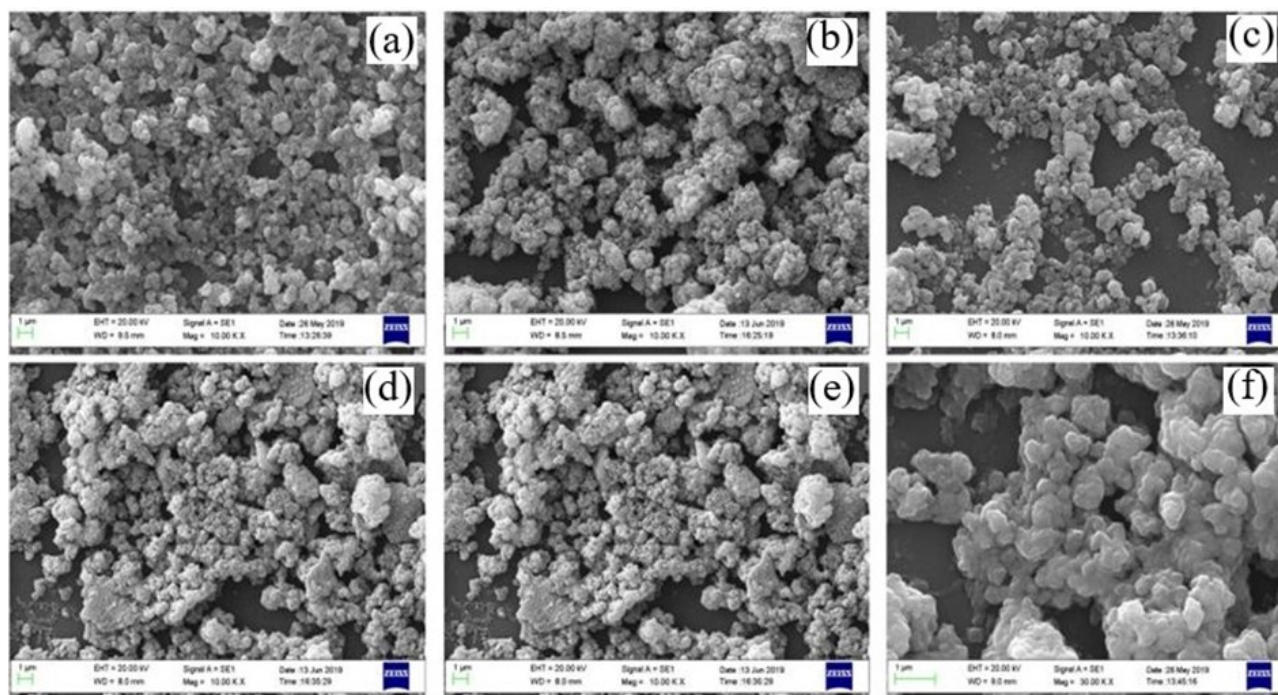
Figure 3. SEM micrographs, (a) Co_3O_4, (b) NiCo (1:2), (C) NiCo (1:1), (d) NiCo (2:1), (e) NiO, and (f) NiCo (1:1) aged at 700 ºC.
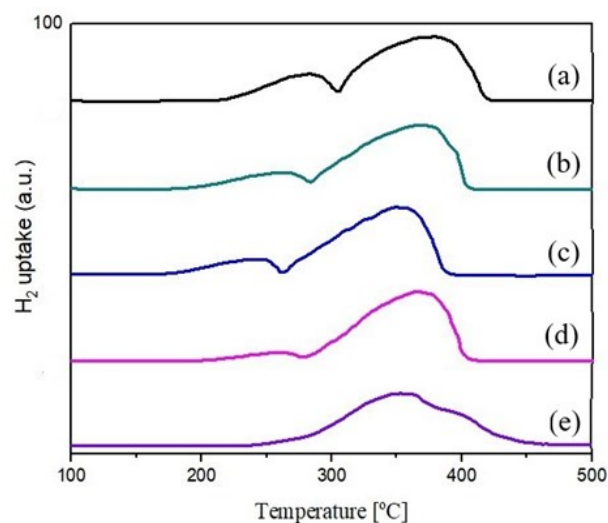
samples tend to absorb moisture physically. The additional broad bands in the region beyond 1100 cm^{-1} indicates the presence of some carbonate species and moisture in the samples [25].

3.3 SEM Characterization Results

The SEM micrographs of all the samples are shown in Figure 3. It is observed that the particles adopted irregular morphology with different sized particle. The particles were spherical and highly agglomerated in nature. The observed bigger particles were made out of agglomeration or overlapping of the smallest nanoparticles.

### 3.4 H$_2$-TPR Characterization Results

The H$_2$-TPR results of all the samples are given in Figure 4. The temperature and H$_2$ consumption corresponding to α and β peak positions are summarized in Table 2. The weak reduction peak at lower temperature is referred to as α peak, and strong reduction peak at higher temperature is referred to as β peak. All

the cobalt-containing catalyst samples exhibited two conjoined reduction peaks (α and β) in the temperature range of 200-400 °C.

The Co$_3$O$_4$ exhibits both low-temperature weak reduction peak (α) and high-temperature strong reduction peak (β) at 272 and 382 °C, respectively, indicating the successive reduction of Co$_3$O$_4$ from Co^{3+} to Co^{2+} and from Co^{2+} to Co^0 [26]. Whereas, the other single oxide NiO has shown only a single high-temperature strong reduction peak (β) at 357 °C, attributed to the reduction of Ni^{2+} to NiO [27]. The actual H$_2$ consumption by these single oxides is very close to the theoretically calculated H$_2$ consumption for the same. It further substantiated the fact that the complete reduction of both the single oxides took place. With the increase in Ni oxide content, the decrease in area under α peak (the portion to the left of the dashed line in the Figure 4) as well as the shift in α peak towards the low temperature was observed, especially seen in case of NiCo (1:1) and NiCo (1:2) catalyst. The lower the reduction temperature, lower the peak area; the higher the reducibility of the catalyst.

Figure 4. H$_2$-TPR profiles of (a) Co$_3$O$_4$, (b) NiCo (1:2), (C) NiCo (1:1), (d) NiCo (2:1), and (e) NiO.
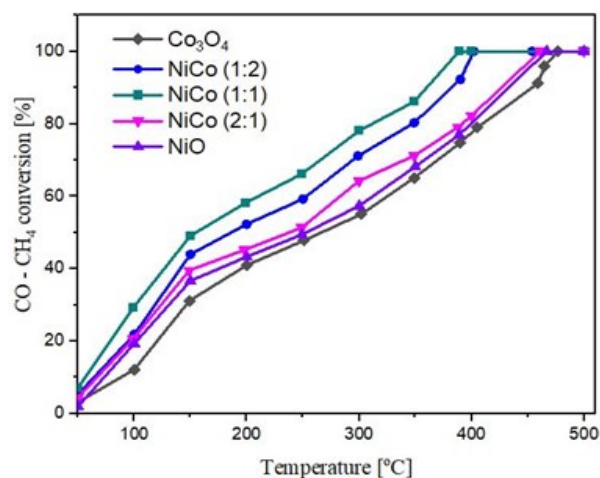
Figure 5. The catalytic activities of Ni-Co bimetal oxides with varying Ni/Co ratios for CO-CH$_4$ mixture oxidation as the function of temperature.

Table 2. Summary of quantitative H$_2$-TPR results of catalysts.

| Catalyst	Peak position (°C)		H$_2$ consumption (mmol.g^{-1})			
	α	β	A	B	$\alpha + \beta$	$\alpha + \beta$ (theoretical)
Co$_3$O$_4$	270	381	3.4	12.1	15.5	16.5
NiCo(1:2)	246	370	2.2	11.8	14.0	15.4
NiCo(1:1)	230	353	2.	11.9	14.0	15.0
NiCo(2:1)	250	367	1.0	12.1		14.4
NiO	-	355		12.25		13.1

As expected, the reducibility order according to the H$_2$ consumption at a lower temperature ($T < 300$ °C) was found to comply with the catalytic performance order exhibited by the catalysts.

3.5 Catalytic Activity

Figure 5 shows the light off curves for CH$_4$ oxidation over all samples along with their corresponding Arrhenius plots for the reaction kinetics. The temperature, T_{90} is the temperature where conversion of the reactants reached 90%, was set as the standard of assessing the activity of the catalysts. The descending order of activity for all the catalysts was as follows: NiCo (1:1) > NiCo (1:2) > NiCo (2:1)> NiO > Co$_3$O$_4$. Arrhenius plots (Figure 5b) also revealed that the NiCo (1:1) catalyst has the lowest calculated apparent activation energy for CH$_4$ combustion. The catalytic activity increased with the increasing Ni content up to the level of molar ratio of NiCo (1:1).

Similarly, Figure 6 showing the light off curves for simultaneous oxidation of CO-CH$_4$ mixture over all the samples shows the same trend as observed in CH$_4$ oxidation. For single oxide catalysts, such as: NiO and Co$_3$O$_4$, the T_{90} were 434 and 459 °C, respectively. Whereas, T_{90} for most NiCo bimetal oxides was lower than 400 °C. Thus, catalytic activity exhibited by NiCo bimetal oxides was much better than that of single metal oxides. The NiCo (1:1) and NiCo (1:2) catalyst achieved the complete conversion of the mixture at 390 and 402 °C, respectively. As clearly indicated in Figure 6 and summarized in Table 3, T_{90} for CO-CH$_4$ mixture is significantly lower in comparison CH$_4$ oxidation over all the studied catalysts. The complete oxidation of CH$_4$ over NiCo (1:1) catalyst took place at 422 °C whereas the complete oxidation of CO-CH$_4$ mixture over NiCo (1:1) catalyst occurred at significantly low temperature of 390 °C. This promoting effect of CO could be possibly due to the highly exothermic nature of the CO oxidation reaction ($\Delta H_r = -282$ kJ.mol^{-1}). The CO gets completely oxidized over NiCo (1:1) catalyst even before the initiation temperature of methane oxidation reaction. The heat released due to CO oxidation locally increases the local temperature, which possibly helps in activating the methane oxidation reaction.
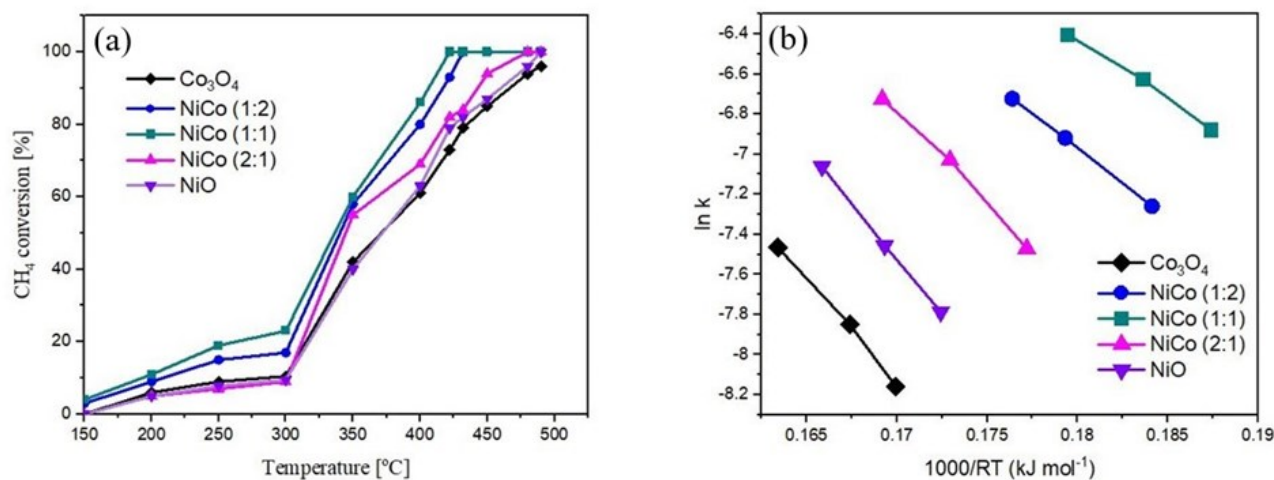
Figure 6. a) The catalytic activities of Ni-Co bimetal oxides with various Ni/Co ratios for CH$_4$ oxidation as the function of temperature; b) the corresponding Arrhenius plots for the reaction kinetics.

Table 3. Summary of characteristic reaction temperatures (T$_{90}$), and apparent activation energy of samples.

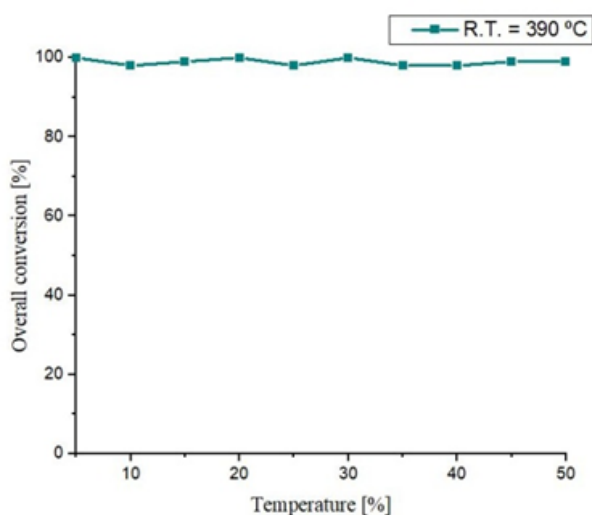| Catalyst	T$_{90}$ (CO+CH$_4$) Mixture (ºC)	T$_{90}$ CH$_4$ Only (ºC)	E$_a$ (kJ mol^{-1})
Co$_3$O$_4$	459	478	124
NiCo (1:2)	382	418	80.6
NiCo (1:1)	380	405	69.4
NiCo (2:1)	428	472	111.7
NiO	434	475	118.3

3.6 Catalyst Stability Test Results

The best performed NiCo (1:1) catalyst was evaluated for its stability under two different methods, as described under section 2.5. The results obtained are as follows:

Time on stream run test: As evident from Figure 7, the catalyst practically exhibited no deactivation and maintained its catalytic performance for a long run of 50 h under the reaction conditions studied, thereby, showing excellent long term stability.

Thermal ageing test: Figure 8 compares the activities of the fresh and aged samples. The catalyst deactivation was practically negligible until the ageing temperature of 600 °C. However, it showed a deactivation after ageing at 700 °C. The conversion dropped to 83% in case of sample aged at 700 °C. This decrease in activity is possibly due to two reasons. Firstly, the thermal decomposition of $NiCo_2O_4$ spinel phase on ageing at 700 °C. Secondly, the increase in crystallite size due to the agglomeration of particles or sintering at high temperatures [28]. As indicated in Figure 1e, in case of sample aged at 700 °C, changes in the diffraction pattern become visible, and high-intensity diffractive peaks of NiO appear. Moreover, the significant agglomeration is observed in the aged sample as compared to the fresh sample in SEM micrographs (Figure 3f), showing increased crystallite sizes. This observation regarding increased crystallite size was also found to comply with the crystalline size calculated from XRD results using Equation (1) (Table 1).
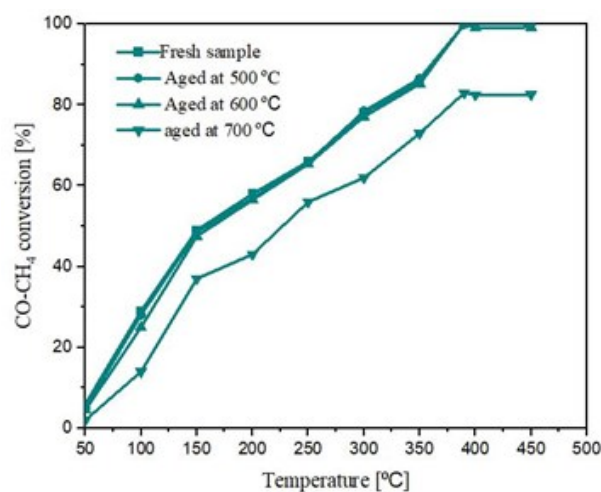
4. Conclusions

The effect of Ni/Co ratio with various nickel content on $CO-CH_4$ mixture oxidation is explained by catalytic activity test and various characterizations like N_2 adsorption-desorption with BET method, XRD, FT-IR, SEM, and H_2-TPR. As per catalytic activity test results, NiCo (1:1) catalyst exhibits the best catalytic performance among all the other observed catalysts. The light-off temperature is shifted towards lower temperatures in the presence of CO. XRD patterns demonstrate that the spinel lattice in the case of NiCo (1:1) is largely distorted compared to other catalysts. The insertion of Ni inappropriate amount causes the disorders in the spinel lattice of cobalt oxides; thereby, enhancing the activity of the reactive ions in the octahedral sites and probably facilitate the dehydroxylation steps, and thus enhancing the catalytic activity of the NiCo bimetal mixed oxides. Further, as evidenced by H_2-TPR results, enhancement in the reducibility of $NiCo_2O_4$ is reported with the structural disorder. Thus, it is concluded that structural disorder in nickel cobaltite spinel phase plays a significant role for the $CO-CH_4$ mixture oxidation.

Acknowledgement

Figure 7. $CO-CH_4$ mixture conversion over NiCo (1:1) catalyst as a function of reaction time at 390 ºC under the reaction conditions.

Figure 8. $CO-CH_4$ mixture conversions as a function of ageing temperature for the fresh, aged at 500 ºC, aged at 600 ºC and aged at 700 ºC NiCo (1:1) catalyst.

Conflict of Interest

The authors declare that they have no conflict of interest.

References

[1] Singha, R.K., Ghosh, S., Acharyya, S.S., Yadav, A., Shukla, A., Sasaki, T., Venezia, A.M., Pendem, C., Bal, R. (2016). Partial oxidation of methane to synthesis gas over Pt nanoparticles supported on nanocrystalline CeO_2 catalyst. *Catalysis Science & Technology,* 6(12), 4601-4615. DOI: 10.1039/C5CY02088C

[2] Lim, T.H., Cho, S.J., Yang, H.S., Engelhard, M.H., Kim, D.H. (2015). Effect of Co/Ni ratios in cobalt nickel mixed oxide catalysts on methane combustion. *Applied Catalysis A: General,* 505, 62-69. DOI: 10.1016/j.apcata.2015.07.040

[3] Trivedi, S., Prasad, R., Gautam, S.K. (2018). Design of active $NiCo_2O_4$-δ spinel catalyst for abatement of CO-CH4 emissionsfrom CNG fueled vehicles. *AIChE Journal,* 64(7), 2632-2646.

[4] Chiew, A.L., Buckley, N.A. (2014). Carbon monoxide poisoning in the 21st century. *Critical Care,* 18(2), 221-221. DOI: 10.1186/cc13846

[5] Balzan, M.V., Agius, G., Galea Debono, A. (1996). Carbon monoxide poisoning: easy to treat but difficult to recognise. *Postgraduate Medical Journal,* 72(850), 470-473. DOI: 10.1136/pgmj.72.850.470

[6] Rosenzweig, A.C. (2015). Biochemistry: Breaking methane. *Nature,* 518(7539), 309-310. DOI: 10.1038/nature14199

[7] Escandón, L.S., Niño, D., Díaz, E., Ordóñez, S., Díez, F.V. (2008). Effect of hydrothermal ageing on the performance of Ce-promoted PdO/ZrO_2 for methane combustion. *Catalysis Communications,* 9(13), 2291-2296. DOI: 10.1016/j.catcom.2008.05.026

[8] Gaur, S., Wu, H., Stanley, G.G., More, K., Kumar, C.S.S.R., Spivey, J.J. (2013). CO oxidation studies over cluster-derived Au/TiO_2 and AUROlite™ Au/TiO_2 catalysts using DRIFTS. *Catalysis Today,* 208, 72-81. DOI: 10.1016/j.cattod.2012.10.029

[9] Mandapaka, R.K., Madras, G. (2015). Kinetics of CO oxidation on palladium using microkinetics coupled with reaction route analysis. *Chemical Engineering Science,* 131, 271-281. DOI: 10.1016/j.ces.2015.03.056

[10] Zhu, X., Du, Y., Wang, H., Wei, Y., Li, K., Sun, L. (2014). Chemical interaction of Ce-Fe mixed oxides for methane selective oxidation. *Journal of Rare Earths,* 32(9), 824-830. DOI: 10.1016/S1002-0721(14)60148-4

[11] Dubey, A., Reddy, K.P., Gopinath, C.S. (2017). Ambient CO Oxidation on In-Situ Generated Co_3O_4 Spinel Surfaces with Random Morphology. *ChemistrySelect,* 2(1), 533-536. DOI: 10.1002/slct.201602010

[12] Cai, T., Yuan, J., Zhang, L., Yang, L., Tong, Q., Ge, M., Xiao, B., Zhao, K., He, D. (2018). Ni−Co−O solid solution dispersed nanocrystalline Co_3O_4 as a highly active catalyst for low-temperature propane combustion. *Catalysis Science & Technology,* 8(21), 5416-5427. DOI: 10.1039/C8CY01062E

[13] El-Kemary, M., Nagy, N., El-Mehasseb, I. (2013). Nickel oxide nanoparticles: Synthesis and spectral studies ofinteractions with glucose. *Materials Science in Semiconductor Processing,* 16(6), 1747-1752. DOI: 10.1016/j.mssp.2013.05.018

[14] Mrowec, S., Grzesik, Z. (2004). Oxidation of nickel and transport properties of nickel oxide. *Journal of Physics and Chemistry of Solids,* 65 (10), 1651-1657. DOI: 10.1016/j.jpcs.2004.03.011

[15] Li, J., Liang, X., Xu, S., Hao, J. (2009). Catalytic performance of manganese cobalt oxides on methane combustion at low temperature. *Applied Catalysis B: Environmental,* 90(1), 307-312. DOI: 10.1016/j.apcatb.2009.03.027

[16] Kan, W.E., Roslan, J., Isha, R. (2016). Effect of Calcination Temperature on Performance of Photocatalytic Reactor System for Seawater Pretreatment. *Bulletin of Chemical Reaction Engineering & Catalysis*, 11(2), 230-237. DOI: 10.9767/bcrec.11.2.554.230-237

[17] Trivedi, S., Prasad, R. (2016). Reactive calcination route for synthesis of active Mn–Co_3O_4 spinel catalysts for abatement of CO–CH4 emissions from CNG vehicles. *Journal of Environmental Chemical Engineering,* 4(1), 1017-1028. DOI: 10.1016/j.jece.2016.01.002

[18] Prasad, R., Rattan, G. (2009). Design of a Compact and Versatile Bench Scale Tubular Reactor. *Bulletin of Chemical Reaction Engineering & Catalysis*, 4(1), 5-9. DOI: 10.9767/bcrec.4.1.1250.5-9

[19] Berger, R.J., Pérez-Ramırez, J., Kapteijn, F., Moulijn, J.A. (2002). Catalyst performance testing: Radial and axial dispersion related to dilution in fixed-bed laboratory reactors. *Applied Catalysis A: General,* 227(1), 321-333. DOI: 10.1016/S0926-860X(01)00950-4

[20] Tabar, A.R., Hamidi, A.A., Ghadamian, H. (2017). Experimental investigation of CNG and gasoline fuels combination on a 1.7 L bi-

fuel turbocharged engine. *International Journal of Energy and Environmental Engineering,* 8(1), 37-45. DOI: 10.1007/s40095-016-0223-3

[21] Matam, S.K., Otal, E.H., Aguirre, M.H., Winkler, A., Ulrich, A., Rentsch, D., Weidenkaff, D., Ferri, D. (2012). Thermal and chemical aging of model three-way catalyst Pd/Al$_2$O$_3$ and its impact on the conversion of CNG vehicle exhaust. *Catalysis Today,* 184(1), 237-244. DOI: 10.1016/j.cattod.2011.09.030

[22] Einaga, H., Kiya, A., Yoshioka, S., Teraoka, Y. (2014). Catalytic properties of copper–manganese mixed oxides prepared by coprecipitation using tetramethylammonium hydroxide. *Catalysis Science & Technology,* 4(10), 3713-3722. DOI: 10.1039/C4CY00660G

[23] Martínez-Arias, A., Fernández-García, M., Ballesteros, V., Salamanca, L.N., Conesa, J.C., Otero, C., Soria, J. (1999). Characterization of High Surface Area Zr−Ce (1:1) Mixed Oxide Prepared by a Microemulsion Method. *Langmuir,* 15(14), 4796-4802. DOI: 10.1021/la981537h

[24] Basahel, S.N., El-Maksod, I.H.A., Abu-Zied, B.M., Mokhtar, M. (2010). Effect of Zr4+ doping on the stabilization of ZnCo-mixed oxide spinel system and its catalytic activity towards N$_2$O decomposition. *Journal of Alloys and Compounds,* 493(1), 630-635. DOI: 10.1016/j.jallcom.2009.12.169

[25] Tharayil, N.J., Raveendran, R., Vaidyan, A.V., Chithra, P. (2008). Optical, electrical and structural studies of nickel-cobalt oxide nanoparticles. *Indian Journal of Engineering & Materials Sciences*, 15(6), 489-496.

[26] Klissurski, D., Uzunova, E., Ivanov, K. (1992). Binary spinel cobaltites of nickel, copper and zinc as precursors of catalysts for carbon oxides methanation. *Catalysis Letters,* 15(4), 385-391. DOI: 10.1007/BF00769162

[27] Parmaliana, A., Arena, F., Frusteri, F., Giordano, N. (1990). Temperature-programmed reduction study of NiO–MgO interactions in magnesia-supported Ni catalysts and NiO–MgO physical mixture. *Journal of the Chemical Society, Faraday Transactions,* 86(14), 2663-2669. DOI: 10.1039/FT9908602663

[28] Istadi, I., Anggoro, D.D., Amin, N.A.S., Ling, D.H.W. (2011). Catalyst deactivation simulation through carbon deposition in carbon dioxide reforming over Ni/CaO-Al$_2$O$_3$ catalyst. *Bulletin of Chemical Reaction Engineering & Catalysis*, 6 (2), 129-136, DOI: 10.9767/bcrec.6.2.1213.129-136.